ACS OMEGA

Open Access



http://pubs.acs.org/journal/acsodf

Article

# Inhibition of the RNA-Dependent RNA-Polymerase from SARS-CoV-2 by 6-Chloropurine Isoxazoline-Carbocyclic Monophosphate Nucleotides

Marco Leusciatti, Beatrice Macchi,* Francesca Marino-Merlo, Antonio Mastino, Giulia Morra,* and Paolo Quadrelli*

Cite This: *ACS Omega* 2023, 8, 36311−36320

Read Online

ACCESS | Metrics & More | Article Recommendations | Supporting Information

**ABSTRACT:** Isoxazoline-carbocyclic monophosphate nucleotides were designed and synthesized through the chemistry of nitrosocarbonyl intermediates and stable anthracenenitrile oxide. Docking and molecular dynamics studies were first conducted for determining the best candidate for polymerase SARS-CoV-2 inhibition. The setup phosphorylation protocol afforded the nucleotides available for the biological tests. Preliminary inhibition and cytotoxicity assays were then performed, and the results showed a moderate activity of the nucleotides accompanied by cytotoxicity.

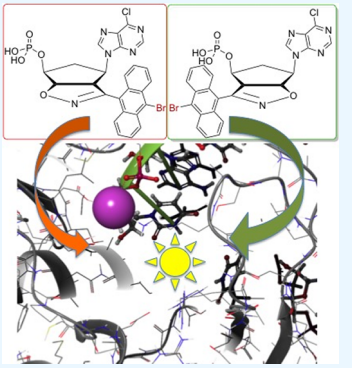

## INTRODUCTION

Over the last three years, we have been experiencing the world health crisis triggered by a devastating pandemic, which challenged us both in public health policies and in pharmacological tools. Starting from the end of 2019, SARS-CoV-2 rapidly spread worldwide since the first localized epicenter in China's Hubei Province, causing COVID-19, a disease associated with a severe form of interstitial pneumonia.[1] The pandemic advanced with exponential growth resulting in millions of cases and deaths.[2,3] With an unprecedented effort, anti-COVID-19 vaccination campaigns started at the end of 2020 in several countries, promising to end the pandemic.[4] Despite vaccination success, a worldwide uneven distribution of doses, vaccine hesitancy in the population, emergence of virus variants, and noticing of limited duration of protective immunity made eradication an unlikely outcome and highlighted the need for efficacious pharmacological treatments.[5−7] Since the beginning of the pandemic, a critical aspect has been the lack of effective antiviral therapeutics to treat COVID-19 patients. Repurpose of antivirals already approved exhibiting inhibitory activity against either proteases (Lopinavir, Ritonavir) or RNA-dependent RNA-polymerases (RdRp) of other viruses (Remdesivir, Favipiravir), was initially proposed as a possible strategy and inspired a number of studies.[8] Nevertheless, it was reported that Remdesivir, Lopinavir, and interferon regimens had little or no effect on COVID-19 hospitalized patients, as indicated by overall mortality, initiation of ventilation, and duration of hospital stay. These various outcomes pushed toward the development of new therapeutics specifically targeted toward SARS-CoV-2. The use of Molnupiravir, prodrug of ß-D-*N*4-hydroxycytidine (from Merck), was approved as a competitive inhibitor of SARS-CoV-2 RdRp[9] and orally active 3C-like protease inhibitor PF-07321332+Ritonavir (Paxlovid, from Pfizer) only for use in patients at high risk of COVID-19 disease progression.[10]

These recent determinations have oriented the development of antiviral drugs targeting RdRp that is an essential enzyme for the viral replication process, catalyzing the viral RNA synthesis using a metal ion-dependent mechanism. An updated overview has reported the main sequence and structural features of the RdRp of emerging RNA viruses such as Coronaviruses, Flaviviruses, and HCV, as well as inhibition strategies implemented so far.[11]

For more than 20 years, we have been investigating the synthetic methodologies in organic chemistry to achieve reliable advancement in the knowledge of chemical structures apt to behave as antiviral compounds to contrast infectious diseases.[12] We strongly promoted the pericyclic reaction

**Received:** July 9, 2023
**Accepted:** September 4, 2023
**Published:** September 20, 2023

approach to several compounds and in particular the exploitation of the chemistry of nitrosocarbonyls, a family of fleeting intermediates suitable for the stereochemical ordinate introduction on carbocyclic scaffolds of functional groups suitable for the linear construction of purine and pyrimidine heterobases as well as introduction of phosphate units.[13]

Nitrosocarbonyl chemistry offers indeed rapid and reliable access to a variety of organic compounds, often capable of remarkable biological activities in different fields. By using this powerful synthetic instrument, we designed a special type of carbocyclic nor-nucleotide in the monophosphate form to conduct a computational analysis aiming to investigate the behavior of selected compounds as possible binders for SARS-CoV-2 RdRp and to verify the relationship between molecular structures and potential activity. Modeling studies will direct/orientate the synthetic strategies and suggest eventual/consequent structural design changes. Second, biological evaluations through antiviral and cytotoxicity tests will give immediate and preliminary responses on the activity of the prepared compounds, providing helpful feedback for concentrating the efforts of modeling and synthesis toward the most promising molecules.

It clearly appears the pivotal combination of these three pillars [modeling⇔chemistry⇔in vitro tests] that are highly connected and integrated and the results of any advancement in one area generate effects in the others in a continuous way, thus fulfilling the application of pericyclic reactions in this Proof of Concept (POC) devoted to contrast SARS-CoV-2.

In fact, Scheme 1 reports the setup chemical design obtained by means of those synthetic instruments which typically

**Scheme 1. Chemical Design of Carbocyclic Nor-Nucleotides**

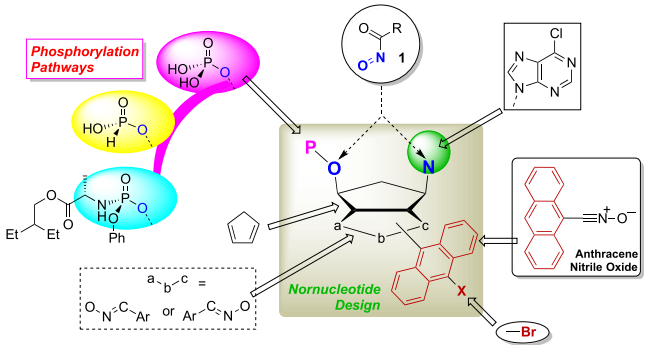


operate in the field of pericyclic reactions: hetero Diels–Alder (HDA) and 1,3-dipolar cycloadditions; in addition, the derivatization of aromatic substituents, the construction of specific heterobases (6-chloropurine) and the choice of the best phosphorylation method will complete the building protocol of the newly proposed antiviral candidates.

The syntheses of the nor-nucleosides start from the hetero Diels–Alder (HDA) cycloaddition of suitably prepared nitrosocarbonyl intermediates **1** and cyclopentadiene, followed by the 1,3-dipolar cycloaddition reaction of the obtained dipolarophile with the stable anthracenenitrile oxide **2** (Scheme 2). The derivatization of the antracene ring with bromine conducted on the regioisomeric cycloadducts and the linear construction of the 6-chloropurine rings will afford the nucleosides of type **3**. These are the precursors of the nor-nucleotides of type **4** that can be obtained through phosphorylation according to properly chosen protocols.

**Scheme 2. General Synthetic Strategy toward Brominated/Phosphorylated Nor-Nucleotides of Type 4**

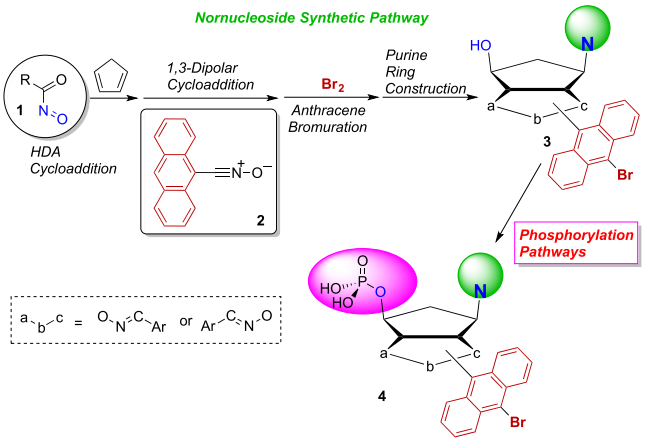


Phosphorylated compounds are essential to conduct first a computational study for determining the best candidate for SARS-CoV-2 inhibition and second to perform the biological assays on viral polymerases.

The study also aims to set the experimental conditions of the new synthetic steps introduced in our nucleoside protocol. In particular, the phosphorylation steps need to become a standard in our pathway. Before these latter steps, the derivatization of the anthracene moiety with bromine, a large atom, modifies the steric demand of the polycyclic system in a specific position; in addition, bromine atom offers the way for further functionalizations on the aromatic ring through simple substitution affording suitably designed more complex derivatives, if needed/suggested by the modeling.

Additionally, the choice of the 6-chloropurine ring as a heterobase allows for the valuable possibility to further functionalize the heterocyclic ring at the position[6] with replacement of the chlorine atom with several nucleophiles (e.g., RR'N, OH, RO, SH, etc.). These reactions can be conducted in mild and efficient ways, thus widening the product family available for different purposes, as the modeling will be able to indicate a better inhibition of SARS or other respiratory viruses.

## RESULTS

**Computational Analysis: Binding Prediction.** *Methods.* Computational experiments were conducted inside Schrodinger's Maestro v13.1.141 release 2022-1.

*Modeling.* Downloaded proteins from the Protein Data Bank (PDB: 7CTT; 7BV2) were prepared by using the Protein Preparation Wizard. Water was removed, hydrogens and missing side chains were added, and the states were generated using Epik at pH 7 ± 2. PROPKA at pH 7 was used for H-bond assignment, and then restrained minimization, with OPLS4 force field to converge heavy atoms to Root-Mean-Square-Deviation (RMSD) of 0.30 Å, was conducted. In the crystal structure of PDB: 7BV2, the diphosphate group and its coordinated magnesium ion were also removed. Remdesivir was modeled detached from chain P. The volume of the binding pocket was calculated using the script *volume_calc.py* provided by Schrodinger.

*Docking.* In order to optimize the size and shape of the binding site, each ligand was initially built starting from the pre-existing crystal ligand in an iteration scheme where protein



https://doi.org/10.1021/acsomega.3c04918
ACS Omega 2023, 8, 36311−36320

minimization steps were performed after adding each new group to accommodate it in the pocket. Finally, the structure was minimized, as described above. In the crystal structure of PDB 7CTT, cytosine residue C 10 was converted to uracil prior to the minimization. Grids for docking were generated using Glide, with default settings. Ligands were built with the 3D Builder tool of Maestro and then prepared with LigPrep using force field OPLS4, and Epik was used to generate possible states at target pH 7 ± 2. Ligands were docked with standard precision in the predefined grids by using Glide. Ten poses per ligand were generated, and postdocking minimization was performed. Optimal poses were chosen based on docking score and base-pairing with the complementary base.

*MD Simulations.* The construct used for the DESMOND simulations of the precatalytic state consists of the 7CTT protein structure complex after removing chain D, residues 22−26 of chain T and residues 5−9 of chain Q to make it comparable to the 7BV2 construct. The system was prepared using Desmond's System Builder with the OPLS4 force field. Protein−ligand complexes or apo proteins (i.e., protein without the prostetic group) were put into an orthorhombic box, surrounded by around 27,000 water molecules and SPC solvent model, with a buffer distance of 10 Å. The volume of the system was then minimized to around $1 \times 10^6$ Å. Negative charges in the system were neutralized by the addition of $Na^+$ ions. NaCl at a concentration of 0.15 M was also added.

Molecular dynamics trajectories were generated by using Schrodinger's Desmond. NPT ensemble was used at a temperature of 300.0 K and pressure of 1.01325 bar. Prior to the simulation, the system was relaxed with the standard relaxation protocol of Desmond with default settings resulting in around 200 ps equilibration. Nose-Hoover thermostat with relaxation time 1 ps and Martyna-Tobias-Klein barostat with relaxation time 2 ps were used. The coupling was set to isotropic. Simulations were run for 50 ns and the trajectory was recorded each 20 ps.

*Trajectory Analysis.* Interactions with the protein and RMSD were obtained through the simulation interactions diagram plugin of Maestro. Hydrogen bonds and distances were calculated using VMD, the protein was first centered in the box, and then frames were aligned. Donor−acceptor distance was set to 3.0 Å and the angle cutoff to 20° in the VMD H-Bond plugin.

Distances in Å were measured throughout the course of the trajectory from the C$\alpha$ of the residue pairs Asp761-Ala550, Asp761-Lys798 and OH3′ of the elongating strand of RNA and P$\alpha$ of the ligand. Mean values are reported.

**Receptor Modeling and Docking.** Chart 1 shows the regioisomeric monophosphate nucleotide structures **4a** and **4b** in their enantiomeric forms that were used for modeling and computational analyses. Since computational studies are conducted on the SARS-CoV-2 RNA polymerase, the monophosphate structures of Chart 1 have been modified as triphosphate derivatives to fit the mechanism of action of nucleotides when interacting with polymerases. Subsequently, the same compounds were re-examined by deleting the pyrophosphate group to restore them in the monophosphate forms, aiming to verify the behavior of simpler derivatives.

The set of the four assumed compounds **4a(1)**, **4a(2)**, **4b(1)**, and **4b(2)** was examined as possible binders for SARS-CoV-2 RdRp by means of a computational strategy combining molecular docking and molecular dynamics (MD) simulations. To this end, two different inhibitor-bound high-resolution

**Chart 1. Chemical Structure of Designed Compounds 4a and 4b, Couples of Enantiomers**

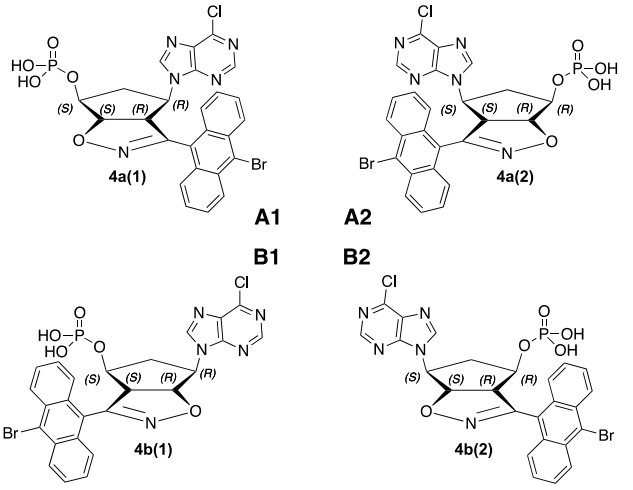


experimental structures of SARS-CoV-2 RdRp were considered as receptors. The first one is the precatalytic state (7CTT.pdb)[22] in complex with the triphosphate form of Favipiravir before incorporation into the chain. The second structure (7BV2.pdb)[23] represents the Remdesivir-bound postcatalytic, pretranslocation state, where the inhibitor has been just incorporated into the primer RNA strand and therefore has lost its pyrophosphate moiety.

The overall volume of the nucleotide binding pocket is only slightly reduced by 20% in the postcatalytic one (see Methods). The nucleotide binding pockets in the pre- and postcatalysis forms mainly differ by the positioning of several positively charged Lys and Arg residues, namely, K551 R553 R555 K621, and K798. In the precatalytic structure 7CTT those residues are oriented to coordinate the negatively charged triphosphate group: despite being limited by the low density map, it is hypothesized that residues R553 and R555 might interact with the $\beta$- and $\gamma$-phosphate groups of Favipiravir triphosphate, while the terminal $\gamma$-phosphate is involved in a salt bridge contributed by K798. These interactions together are hypothesized to stabilize the incoming nucleotide and 3′ terminus of primer RNA in close vicinity to facilitate the nucleophilic attack.

Hence, this structure allows us to investigate the recognition of the triphosphate form of the designed compounds and generate hypotheses about the possibility of incorporating them into the chain. In contrast, in the postcatalytic structure 7BV2, which still contains the pyrophosphate after the incorporation reaction, the positively charged residues are far away from the pyrophosphate as its negative charge is partially neutralized by the proximity of the second $Mg^{2+}$ ion.

This structure, after modeling the detachment of the nucleotide analogue ligand from the RNA chain and deleting the pyrophosphate group, is used to test by molecular docking the binding of the monophosphate form of each compound in parallel to targeting 7CTT. Also, the docking of the monophosphate form of each compound in the postcatalytic structure can cross validate the binding pose found for its triphosphate form, under the hypothesis that chain incorporation might take place.

Each one of the four ligands was docked to each one of the structures, either in triphosphate (to 7CTT) or in monophosphate form (to 7CTT and 7BV2). To be able to pair



https://doi.org/10.1021/acsomega.3c04918
ACS Omega 2023, 8, 36311−36320

Remdesivir starting from the Favipiravir bound structure, a mutant C → U was modeled in the complementary base of template RNA of 7CTT. The matrix of receptor−ligand pair combinations was used to generate a set of complex models, which are filtered in terms of docking score and pose.

Due to the bulky character of the anthracene moiety, for each ligand, the binding site was first relaxed by gradually growing the compound inside the pocket and correspondingly minimizing the local environment, and then, once equilibrated, the compound was removed and rigid docking was performed (see Methods).

Docking poses were first evaluated by comparing the normalized binding energy (or ligand efficiency) to the native ligands Favipiravir or Remdesivir and then by inspecting the presence of base pairing between the 6-chloropurine moiety and the complementary base. The correct positioning of the triphosphate is also considered an evaluation criterion.

Figure 1 shows the docking poses of the enantiomeric couples of compounds **4a** and **4b** in their *triphosphate* forms.

The results of the docking experiment reveal that **4a(2)** (Figure 1, **A2**) docked to 7CTT shows the best arrangement in terms of both geometry, when compared to the reference ligand Favipiravir, and ligand efficiency. Table S1 in the Supporting Information (SI) reports the ligand efficiencies of selected binding poses of the triphosphate derivatives in the precatalytic structure. In **4a(2)**, the anthracene moiety interacts through stacking with the n-1 base, while the 6-chloropurine moiety is engaged in base pairing to the template RNA (Figure S1 in the SI).

In contrast, for compound **4a(1)** (Figure 1, **A1**) no pose was found, showing a correct base pairing in either receptor structure. Also, no $\pi$-stacking interactions are formed by the anthracene group, which cannot be accommodated in the pocket (see Figure S1 in the SI). This compound was therefore discarded in the following analysis.

Compounds **4b(1)** and **4b(2)** (Figure 1, **B1** and **B2**) show different arrangements in their triphosphate form docked to target 7CTT. On the one hand, **4b(2)** keeps the anthracene group in a stacking interaction with base n-1 but abolishes the base pairing by the 6-chloropurine moiety. Conversely, triphosphate **4b(1)** does not establish any stabilizing interactions apart from the phosphate group (see also Figure in the SI).

Figure 2 shows the selected binding poses of enantiomeric couples **4a** and **4b** in the *monophosphate* forms docked to 7BV2 (see also Figure S2 in the SI).

In pose **A1** of Figure 2, the anthracene ring in compound **4a(1)** is located erratically in the position normally occupied by the heterobase, presenting a $\pi$-stacking with base n-1; the phosphate group is coordinated to the $Mg^{2+}$ ion, also coordinated by the oxygen atom belonging to the isoxazoline ring. The 6-chloropurine ring of **4a(1)** is orientated toward the loop where the Ala550 is located.

Analogously, **4a(2)** in the monophosphate form behaves as its corresponding triphosphate, with the anthracene ring positioned under the elongating RNA chain while the 6-chloropurine ring is correctly located, although in the absence of base-pairing. Again, the monophosphate group is coordinated to the $Mg^{2+}$ ion.

Interestingly though, the monophosphate form of **4b(1)** docked to 7BV2 shows coordination of the monophosphate to the catalytic $Mg^{2+}$ ion, correct base pairing, and $\pi$-stacking with base n-1 while the anthracene moiety fills the now available triphosphate subpocket (Figure 2, **B1**). This suggests a possible binding mode of this compound that would be compatible with a non-nucleosidic reverse transcriptase inhibitors (NNRTI) mechanism.

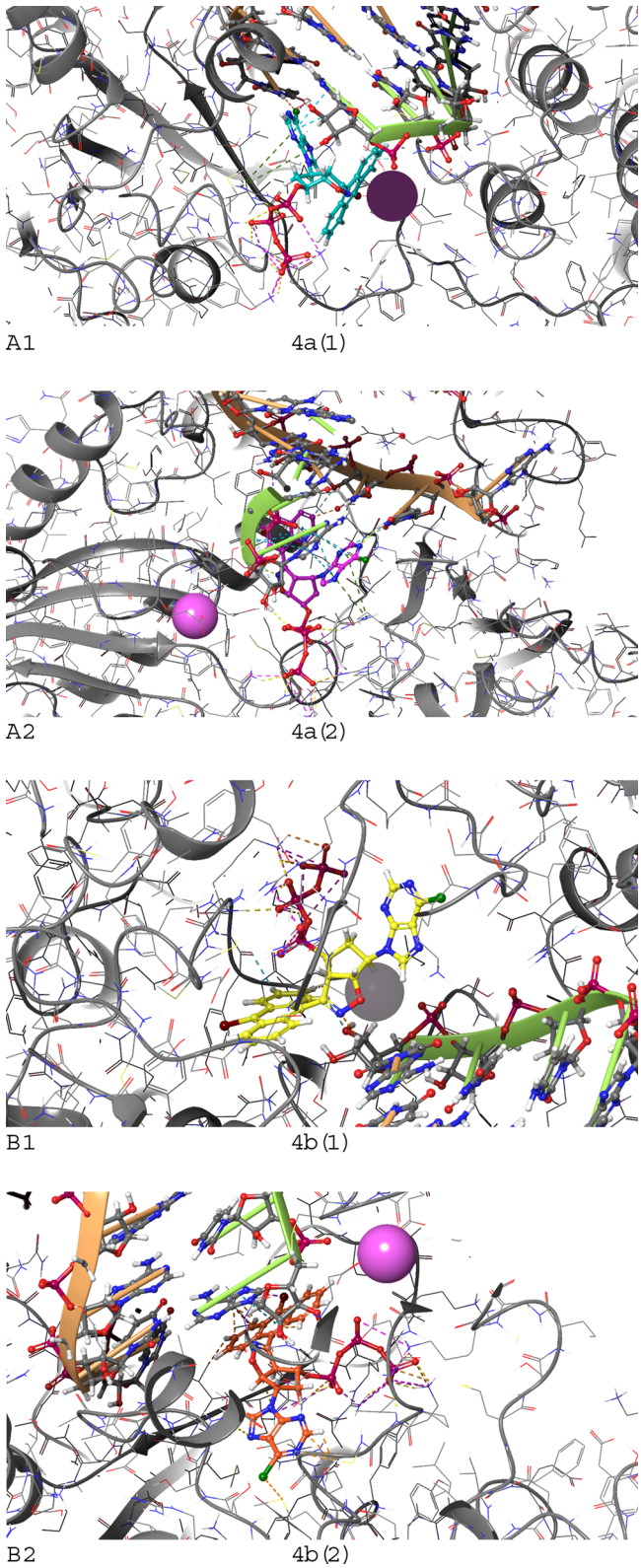


**Figure 1.** Docking poses (**A1,2**, **B1,2**) of enantiomeric compounds **4a** and **4b** in the *triphosphate* forms in the precatalytic structure.



https://doi.org/10.1021/acsomega.3c04918
*ACS Omega* 2023, 8, 36311−36320

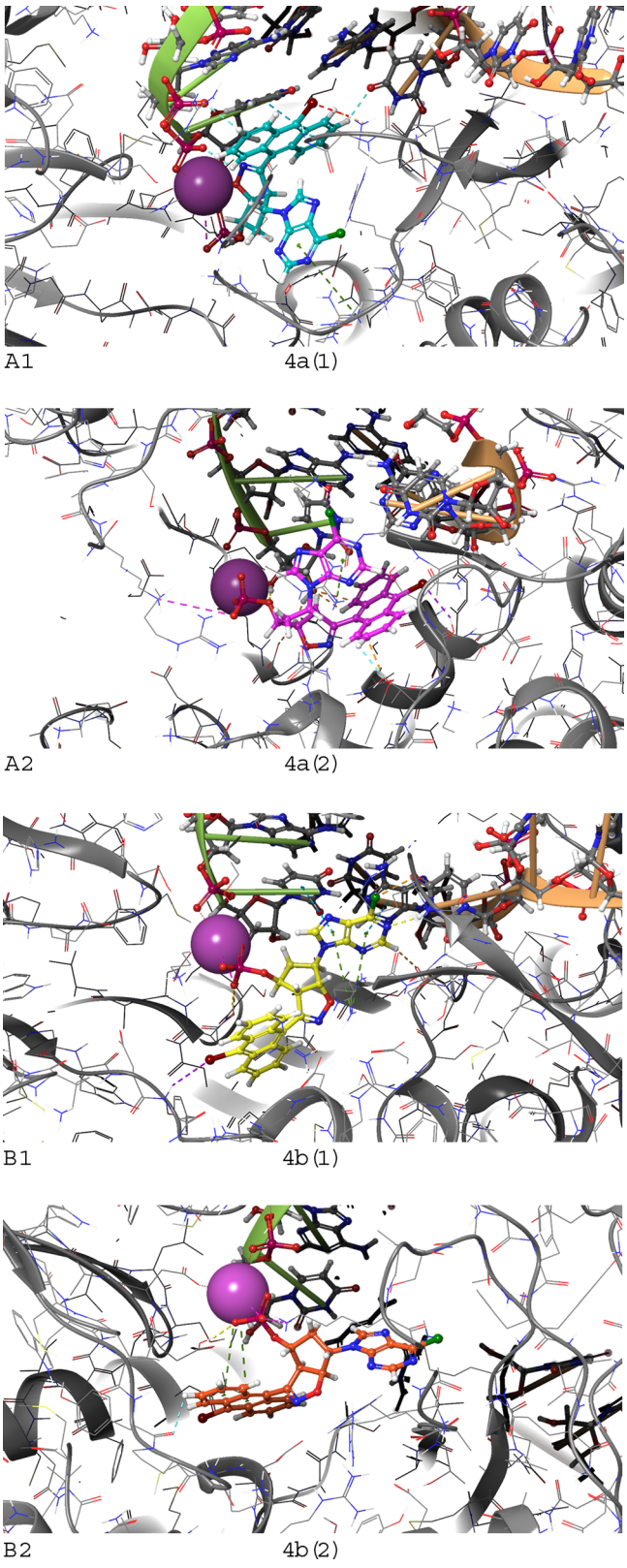


**Figure 2.** Docking poses (**A1,2**, **B1,2**) of enantiomeric compounds **4a** and **4b** in the *monophosphate* forms in the postcatalytic structure.

Finally, in compound **4b(2)** (Figure 2, **B2**) the 6-chloropurine ring is completely out of the pocket; there is a void space where the base should be positioned, but the base misses the target. Furthermore, the anthracene is somewhat hung out in an empty zone thinly connected to the $Mg^{2+}$ ion.

On the basis of the computational results reported above, the structures of compounds **4a(2)** and **4b(1)** will be considered in terms of molecular dynamic studies.

**Molecular Dynamics.** *Triphosphate* and *monophosphate* forms of compounds **4a(2)** and **4b(1)** in complex with RdRp in the precatalytic and the postcatalytic states were further analyzed by means of Molecular Dynamics.

To assess possible local structural rearrangements in the protein, we focused on the closure of the binding pocket by measuring the average distances between the C$\alpha$ atoms of selected residue pairs along the dynamics.

Complexes with **4b(1)** and **4a(2)** were compared to Favipiravir and Remdesivir complexes and the apo form of RdRp and subjected to control MD simulations. Specifically, the distances between Asp761 and Lys798, residues of a $\beta$-sheet responsible for the coordination of the $Mg^{2+}$ ions and the triphosphate group of the incoming nucleotide, and the distance between Asp761 and Ala550, residues contained in the so-called finger of RdRp, were measured (Figure 3, Scatter plot).

MD trajectories (50 ns) were run, and a few parameters were evaluated. Specifically, the RMSD of the ligand was calculated, and the persistence of base pairing was analyzed focusing on Watson−Crick base pairs hydrogen bonding patterns to complementary RNA. For the triphosphate forms complexed to 7CTT the angles are **4a(2)** 55.2° and **4b(1)** 107.8°, respectively. In Favipiravir triphosphate (FTP) the angle is 135.4° between OH3′, the phosphate P$\alpha$ and the pyrophosphate group along dynamics and can suggest how well the nucleotide analogue is positioned for the nucleophilic attack of the OH3′ moiety. **4b(1)** is closer to the reference values for FTP, which suggests a better positioning.

In the 7CTT scatter plot (Figure 3a) the pose **B1** relative to compound **4b(1)** is located in the control zone, while pose **A2** relative to compound **4a(2)** shows a Asp761−Lys798 distance >1 Å. In 7BV2 both compounds are located in the control group (Figure 3b).

The results are summarized in Table S2 in the SI. While **4a(2)** shows a low RMSD (average 1.33 Å) and a reasonably low mean distance between OH3′ and the phosphate (4.7 Å), **4b(1)** shows increased mobility, higher RMSD (3.78 Å) and the phosphate group is displaced away from the position required for catalysis (8.8 Å distance OH3′-P$\alpha$) although, similarly to **4a(2)**, it retains contact to the positively charged residues that coordinate the phosphate group in the Favipiravir crystal structure K551 R553 R555 K621 and K798 (see Figure 3c).

The triphosphate forms of **4a(2)** and **4b(1)** ligands cause the binding pocket parameters to assume the same range of values that are found in the presence of the reference ligands Remdesivir and Favipiravir, which determine a closure of the pocket when compared to the crystal structure values. In contrast, the apo state of both 7CTT variants with uracile and cytosine leads to a wider pocket.

The monophosphate forms were simulated in complex with the postcatalytic structure 7BV2. The same parameters were evaluated here to predict the stability of the poses (see Table S2 in the SI). Results show that monophosphates **4a(2)** and **4b(1)** confirm what was found in the docking experiments. Namely, while **4b(1)**, which had a better ligand efficiency when docked to 7BV2, stably maintains base pairing and an


https://doi.org/10.1021/acsomega.3c04918
ACS Omega 2023, 8, 36311−36320

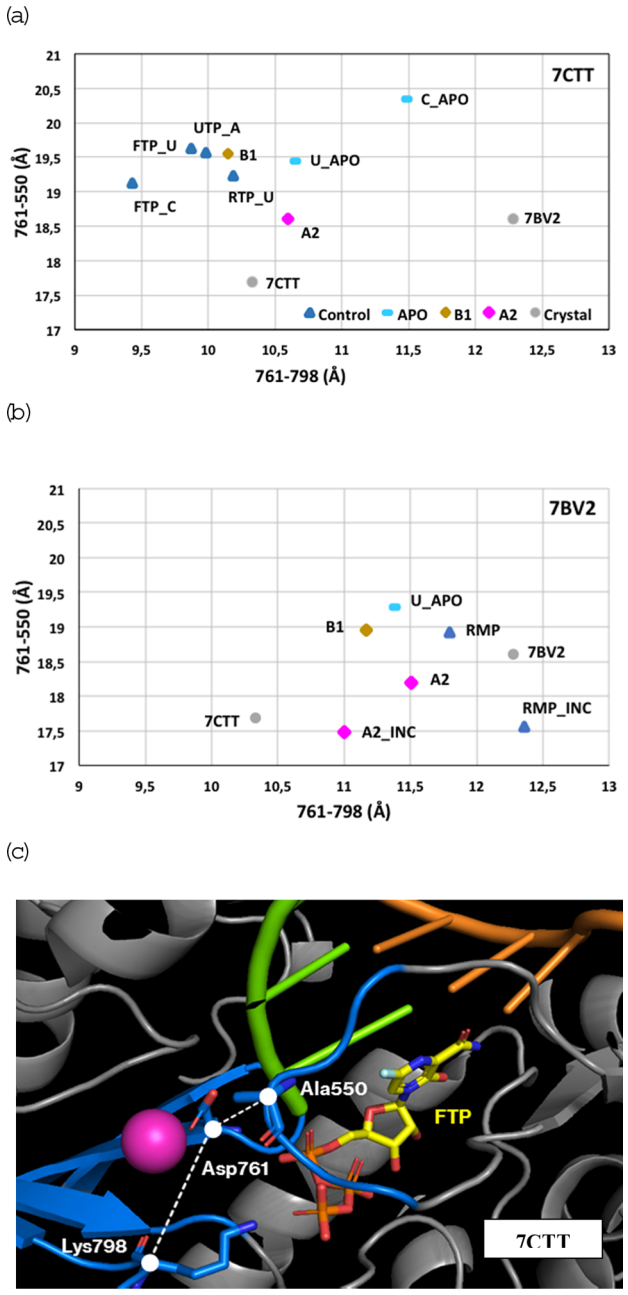


**Figure 3.** Closure of the binding pocket observed in the MD simulations. Scatter plot of the average distances between Asp 671 and Lys 798 and the distance between Asp 761 and Ala 550 in (a) complexes obtained with the 7CTT structure and (b) 7BV2 (refer to Chart 1 for structures). The label 'Control' indicate average for MD simulations of the X-ray complex structures of Remdesivir and/or Favipiravir bound RdRp. These are (a) FTP bound complex with C or U as complementary base; RTP bound complex with U as complementary base. (b) RMP bound complex; RMP bound complex after incorporation into the chain. The pdb code label indicates crystal structure values as further reference. (c) RdRp in complex with FTP in 7CTT.

overall low RMSD, **4a(2)** loses its pairing, reflecting the less favorable binding pose. It is worth mentioning that monophosphate **4a(2)** docked to the precatalytic structure despite the absence of the triphosphate group is able to maintain favorable interactions with the RNA showing a ligand efficiency of −0.317, comparable to the best binders of the target (see SI). On the other hand, the pocket distances (Figure 3) reveal a conformational response of the protein in line with the control ligands monophosphate Remdesivir and Favipiravir, similarly to what is observed in the triphosphate form, resulting in a closer binding pocket than the apo state, as expected.

Overall, this analysis predicts that among the pool of designed compounds, **4a(2)** and **4b(1)** are the ones that could, with different binding modes, productively interact with RdRp. Specifically, for the first one, we expect that both the triphosphate and the monophosphate forms might be active, while for the second one, the monophosphate form shows the best results, due to the occupation of the triphosphate subpocket by the anthracene group. With this ranking in mind, we proceeded with the synthesis of the monophosphate compounds **4a** and **4b** and in vitro testing as a preliminary evaluation of the biological activities in view of further implementation of the synthetic process.

**Chemistry.** The starting regioisomeric compounds were prepared, according to the published procedure,[14] from the *N*-benzoyl-2,3-oxazanorborn-5-ene as dipolarophile in the presence of a slight excess of anthracenenitrile oxide **2** and isolated in nearly 1:1 ratio by column chromatography. The bromination protocol was adapted from the literature procedures[15] and the regioisomeric cycloadducts **3a,b** were obtained as bromo-derivatives upon treatment with bromine under mild conditions (DCM, at reflux for 24 h).

The following synthetic steps run again through the classical pathway (see Notes) required for the linear construction of purine heterobases as we have shown in previous works[13] with few adaptations and experimental improvements. Alkaline hydrolysis[13,16] of the cycloadducts **3a,b**, conducted with grinded NaOH in methanol solutions, afforded the corresponding hydroxylamine derivatives in nearly quantitative yield (Scheme 3).

Hydrogenolysis[13,16] of the hydroxylamine derivatives under standard conditions ($H_2$, Pd/C 10%, AcOEt) afforded the desired aminols **5a,b** (yields: 98 and 97%, respectively).

By using known procedures for the construction of the purine nucleus,[17,18] the aminols **5a,b** were converted into the 6-chloropurine derivatives **6a,b** by substitution of 5-amino-4,6-dichloropyrimidine followed by acid-catalyzed condensation with ethyl orthoformate (Scheme 3).

Finally, the conversion of the nor-nucleosides **6a,b** into the corresponding monophosphate derivatives **4a,b** has been selected among the proposed methods shown in Scheme 2 since these structures represent valuable starting compounds for the synthesis of the relative triphosphate compounds; furthermore, tests are also available for conducting biological evaluation also in the monophosphate derivatives as preliminary evaluation. Hence, we setup the methodology for converting the nucleosides **6a,b** into the regioisomeric monophosphates **4a,b** by adapting the known methods reported in literature.[19,20]

Treatment of the nucleosides **6a,b** with excess $POCl_3$ (3 equiv) in an ice-cooled solution of trimethyl phosphate afforded the desired products **4a,b** in nearly quantitative yield after an overnight reaction at room temperature (Scheme 3).

The obtained products were fully characterized spectroscopically. In the $^1$H NMR (DMSO), the structures of the nucleosides are confirmed upon comparison with the spectra of the starting material. Significantly, the absence of the signal


https://doi.org/10.1021/acsomega.3c04918
ACS Omega 2023, 8, 36311−36320

**Scheme 3. Syntheses of Regioisomeric Nor-Nucleotides of Type 4a,b**

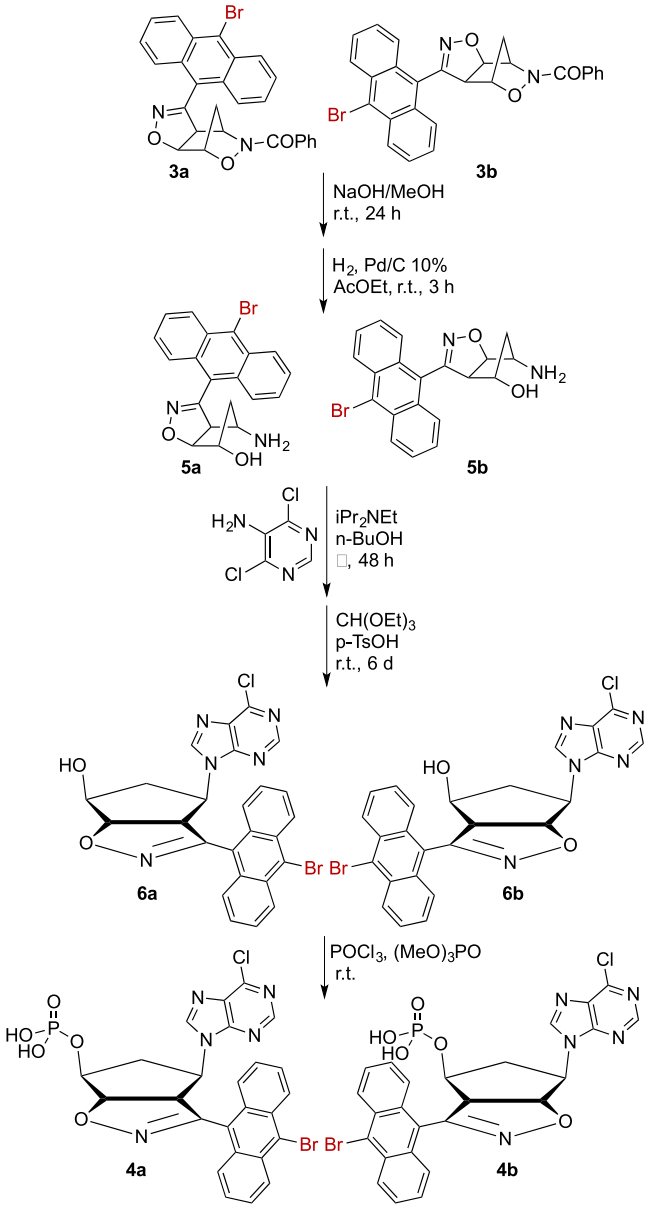


relative to the OH group indicates functionalization with the phosphorus. The $^{31}$P NMR spectrum (DMSO) revealed the presence of the phosphate group as a singlet at $\delta$ −0.10 ppm for compound **4a** and at $\delta$ −2.10 ppm for compound **4b**, in full accordance with the literature on phosphorus derivatives.[21]

**Biological Assays.** Samples of the synthesized monophosphate compounds **4a** and **4b**, representative of the regioisomeric families (**A**) and (**B**) (see Chart 1), were biologically assayed to preliminarily assess their potential as antiviral compounds capable of inhibiting SARS-CoV-2 RdRp activity.

For this purpose, first their cytotoxicity was assayed in terms of inhibition of cell viability and of cell metabolic activity in epithelial HEp-2 and HepG2 cells. Cell viability and death were evaluated by the classical trypan blue assay. The cell metabolic activity was detected through formazan product formation, using a commercial colorimetric kit (MTS [3,4-(5-dimethylthiazol-2-yl)-5-(3-carboxymethoxyphenyl)-2-(4-sulfophenyl)-2H-tetrazolium salt]). Concerning the cell viability, a dose effect assay using three different concentrations of the compounds, within the range from 100 to 0.1 $\mu$M, assessed levels of cytotoxicity, expressed as $CC_{50}$.

Results showed that the **4b** was endowed with a higher ability to induce cell death with respect to **4a** toward both cell lines tested, with $CC_{50}$ values of about 22 $\mu$M for HEp-2 and HepG2 cells (Figure 4a,b). Conversely, **4a** and **4b** compounds,

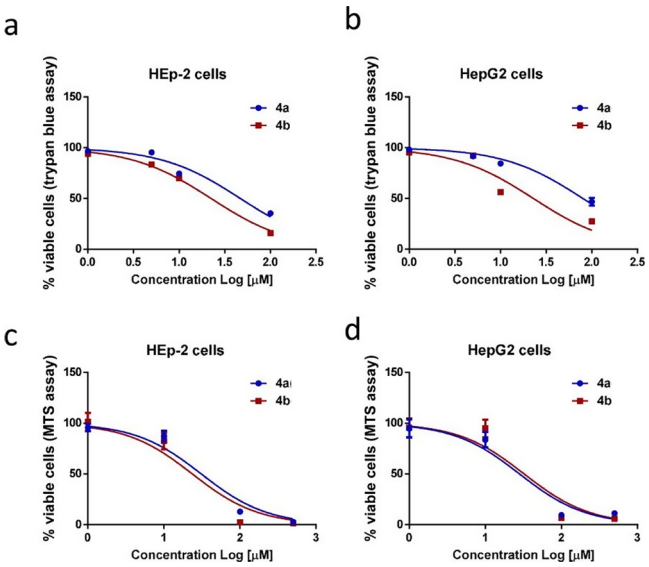


**Figure 4.** Inhibition of cell viability assessed by the trypan blue assay (a, b) and of metabolic activity assessed by MTS assay (c, d) in HEp-2 cells (a, c) and HepG2 cells (b, d) treated with nucleotides **4a** and **4b** for 24 h (experiments in triplicate). Cytotoxicity, calculated as concentration of compounds needed to reduce the viability or metabolic activity by 50% with respect to control cells. $CC_{50}$ values (expressed as mean ± SD: (a) **4a** = 46.79 ± 1.18, **4b** = 22.36 ± 1.04; (b) **4a** = 79.67 ± 1.10, **4b** = 22.85 ± 1.19; (c) **4a** = 30.96 ± 1.2, **4b** = 23.64 ± 1.3; (d) **4a** = 28.14 ± 1.3, **4b** = 32.37 ± 1.4.

assayed within the range from 500 to 1 $\mu$M, showed a quite similar ability in inhibiting the metabolic activity, with **4b** being **4b** more effective toward HEp-2 cells, but not toward HepG2 cells, with respect to **4a** (Figure 4c,d). In any case, even in this assay, the lower $CC_{50}$ value obtained was about 23 $\mu$M for **4b** toward HEp-2 cells (Figure 4c,d).

Thus, the comparative analysis of the cell viability and of the cell metabolic activity inhibition indicated that the two compounds tested, in their current structure, were endowed with a certain cytotoxicity at concentrations higher than 20 $\mu$M (Figure 5). We then focused our attention on the capacity of the compounds to inhibit the SARS-CoV-2 RdRP activity in the range from 10 to 0.01 $\mu$M. For this purpose, a commercial, virus-cell-free assay based on detection of the RNA molecules synthesized by the SARS-CoV-2 recombinant RNA polymerase complex in the presence of an RNA template and NTPs, was utilized. The results showed that **4a** and **4b** were actually capable of significantly reducing RNA synthesis by part SARS-CoV-2 RdRP by about 18 and 25%, respectively, but only at the higher concentration assayed of 10 $\mu$M.

Overall, the results of the biological assays experimentally confirmed what was predicted by the computational analysis about the capability of the newly synthesized nor-nucleotides to efficiently interact with the functional activity of SARS-CoV-2 RdRp, making **4b** more interesting for future design of


https://doi.org/10.1021/acsomega.3c04918
ACS Omega 2023, 8, 36311−36320

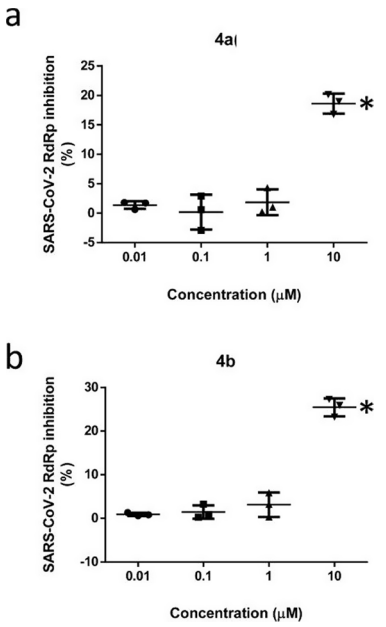


**Figure 5.** Inhibition of SARS-CoV-2 RdRp activity by nucleotides (a) **4a** and (b) **4b**, assessed by a cell/virus-free fluorometric RdRp activity assay. Data presented as the mean ± SD. Statistical significance analyzed using the 1 way ANOVA Bonferroni's multiple comparisons test: $*p < 0.001$ vs all (experiments in triplicate). Inhibitory activity was calculated as the concentration of compounds needed to reduce RdRp activity by 50%. $IC_{50}$ values, expressed as mean ± SD, were: **4a** = 43.83 ± 1.07; **4b** = 29.31 ± 1.05.

structural modifications. On the other hand, the results indicated that the currently designed structure of the compounds is also endowed with a quite high cytotoxic potential.

These drawbacks must be taken into account in relation to the use of isoxazoline-carbocyclic synthetic protocol as the strategic way to select the candidates for the SARS-CoV-2 polymerase inhibition.

## DISCUSSION AND CONCLUSIONS

In this POC study, we have synthesized the regioisomeric nucleosides **6a,b** obtained through the chemistry of nitrosocarbonyl intermediates of type **1**, taking advantage of the use of the stable anthracenenitrile oxide **2**. The synthetic pathway relies upon a well-established protocol, setup in our laboratories and well-documented in several papers and reviews.[12,13] These methodologies are potentially suitable for introducing the phosphorus moiety needed for the biological tests on SARS-CoV-2 polymerases.

We also considered various phosphorylation methods to be applied to functionalize compounds **6a,b**. Among the phosphorylation methods, we set up the experimental conditions to a fast track to monophosphate derivatives through $POCl_3$ treatment, which is the preliminary step for eventual triphosphorilation. The phosphorylation processes gave valuable and reliable results and are pivotal in our strategy oriented to the selection of the best candidate as antiviral compound and specifically dedicated to the contrast of the SARS-CoV-2 virus or other viral emerging infectious diseases. Regarding the SARS topic, a first evaluation has been performed through docking computational studies. Although the nature of nucleoside/nucleotides analogs, they resemble NNRTI that have not yet been found/synthesized to contrast SARS-CoV-2. In principle, they could recognize allosteric nsp12 sites and interact with sites other than those occupied by Remdesivir. NNRTI are considered potential targets by those molecules inducing little cell death since they should be antiviral and not antitumor candidates.[24] The computational studies revealed the possibility for compounds of types **4a** and **4b** to give positive responses in terms of contrast to SARS-CoV-2, with compounds of type **4b** being the most promising.

The biological results showed that **4a** and **4b** were capable of significantly reducing RNA synthesis by part SARS-CoV-2 RdRP by about 18 and 25%, respectively. One of the main problems concerns the concentration required to obtain these performances (10 $\mu$M). Overall, the results of the biological assays confirmed what predicted by the computational analysis. Nevertheless, the results indicated that the currently designed structures of monophosphate compounds are endowed with a quite high cytotoxicity.

Prominent in the current stage of drug development, antiviral compounds can be efficiently prepared through cycloaddition reactions. In recent reviews we reported the use of 1,3-dipolar cycloaddition reactions of selected 1,3-dipoles, from azides[25] to nitrones, passing through nitrile oxides and other ylides,[26] in the light of their application for the preparation of key intermediates in the design and synthesis of compounds that were tested for their antiviral activities against a variety of viruses. The products obtained from these pericyclic reaction approaches were tested for their activities in terms of blocking the virus replication, and the relevant biological data are highlighted.

The ability of the 1,3-dipolar cycloaddition reactions and the hetero Diels–Alder cycloadditions of nitrosocarbonyl intermediates (easily obtained from nitrile oxides through mild oxidation) to produce a variety of heterocyclic scaffolds extends its importance to many areas of organic synthesis, and the synthesis of antiviral compounds represents a topic in constant growing. The use of 1,3-dipoles offers a unique method for the preparation of a variety of compounds with potential biological activity. It must be taken into account that heteroatom-containing cycloadducts may be transformed in other functionalized molecules, cyclic or acyclic. Furthermore, the ability of the 1,3-dipole to generate rings even containing stereocenters in a single synthetic operation is a pivotal step when a valuable compound has to be prepared.

In conclusion, these are surely precious synthetic methods that can be applied for the preparation of antiviral candidates targeting respiratory viruses, SARS-CoV-2 included. The computational screening is also a pivotal step in selecting the most relevant structures, but the biological assays will definitively direct the synthesis toward the desired goal.

The chemistry of pericyclic reactions is still at work!

## EXPERIMENTAL SECTION

**General.** All melting points (mp) are uncorrected. $^1H$, $^{13}C$, and $^{31}P$ NMR spectra were recorded on a 300 MHz spectrometer (solvents specified). Chemical shifts are expressed in ppm from internal tetramethylsilane ($\delta$), and coupling constants ($J$) are in Hertz (Hz): b, broad; s, singlet; bs, broad singlet; d, doublet; t, triplet; q, quartet; m, multiplet. IR spectra (nujol mulls) were recorded on a spectrophotometer available at the Department and absorptions ($\nu$are in $cm^{-1}$. HRMS were done on a X500B QTOF system (Sciex, Framingham, MA 01701 USA) available at the CGS of the University of Pavia. Column chromatography and tlc: silica gel


https://doi.org/10.1021/acsomega.3c04918
ACS Omega 2023, 8, 36311−36320

H60 and $GF_{254}$, respectively; eluants: cyclohexane/ethyl acetate 9:1 to pure ethyl acetate.

*Starting and Reference Materials.* Compounds **3a,b** were synthesized according to the procedure reported in the literature.[14,16,17] Other reagents and solvents were purchased from chemical suppliers and used without any further purification following or adapting the methods reported in the cited literature.

**Synthesis of Nucleotide 4a,b.** To an ice-cooled solution of $POCl_3$ (0.45 mmol) in trimethyl phosphate (0.50 mL) were added nucleosides **6a,b** (80 mg, 0.15 mmol) were added. The resulting solutions were left under stirring at room temperature overnight. After this period of time, the reactions were then diluted with diethyl ether (50 mL) and water was added (50 mL); upon shaking solid compounds precipitate and allowing for their collection by filtration under vacuum. The solid crude products **4a,b** were recrystallized from ethanol/water and fully characterized.

*Compound **4a**.* 80.2 mg (87%), mp 220 °C (dec) from ethanol/water.

IR: $\nu$ = 3245 (OH), 1582 (C═N) $cm^{-1}$.

$^1$H NMR (300 MHz, DMSO-d6, 25 °C): $\delta$ = 2.40 and 2.57 (m, 1H+1H, $CH_2$), 4.61 (bs, 1H, CH-N), 4.79 (m, 1H, CH−O), 5.10 (d, 1H, $J$ = 8 Hz, $H4_{Isox.}$), 5.54 (d, 1H, $J$ = 8 Hz, $H5_{Isox.}$), 7.75 (m, 4H, arom.), 8.15 (m, 4H, arom.), 8.57 (s, 1H, CH═N), 8.77 (s, 1H, CH═N).

$^{13}$C NMR (75 MHz, DMSO-d6, 25 °C): $\delta$ = 37.8, 57.2, 63.3, 76.6, 92.2, 123.1, 124.5, 124.7, 125.4, 125.6, 127.3, 127.6, 128.1, 128.8, 129.3, 129.5, 130.5, 130.7, 146.1, 148.4, 150.3, 151.0, 154.2.

$^{31}$P NMR (121.5 MHz, DMSO-d6, 25 °C): $\delta$ = −0.10 [s, -PO(OH)$_2$].

$C_{25}H_{18}BrClN_5O_5P$ (614.78): HRMS: calcd. (MW-H) 611.9845; found 611.9836.

*Compound **4b**.* 89.5 mg (97%), mp >250 °C (dec.) from ethanol/water.

IR: $\nu$ = 3265 (OH), 1582 (C═N) $cm^{-1}$.

$^1$H NMR (300 MHz, DMSO-d6, 25 °C): $\delta$ = 2.46 and 2.68 (m, 1H+1H, $CH_2$), 4.15 (bs, 1H, CH-N), 4.56 (d, 1H, $J$ = 8 Hz, $H4_{Isox.}$), 5.48 (bs, 1H, CH−O), 6.04 (dd, 1H, $J$ = 8, 2 Hz, $H5_{Isox.}$), 7.81 (m, 4H, arom.), 8.15 (m, 2H, arom.), 8.59 (d, 2H, arom.), 8.88 (s, 1H, CH═N), 8.90 (s, 1H, CH═N).

$^{13}$C NMR (75 MHz, DMSO-d6, 25 °C): $\delta$ = 38.2, 61.7, 67.2, 72.9, 89.3, 123.6, 124.6, 125.7, 127.3, 127.7, 128.3, 128.9, 129.1, 130.8, 131.1, 146.7, 151.6, 151.9, 155.4.

$^{31}$P NMR (121.5 MHz, DMSO-d6, 25 °C): $\delta$ = −2.10 [s, -PO(OH)$_2$].

$C_{25}H_{18}BrClN_5O_5P$ (614.78): HRMS: calcd (MW-H) 611.9845; found 611.9836.

**Biological Assays.** Human larynx epithelial HEp-2 cells (ATCC CCL-23) and human hepatocellular carcinoma cell line HepG2 (ATCC HB-8065), originally obtained from American Type Culture Collection (ATCC, Manassas, VA, USA) were maintained in 10% fetal bovine serum (FBS), 100 units/mL penicillin, 100 mg/mL streptomycin, and 2 mM L-glutamine supplemented RPMI 1640 (all from Euroclone, Milan, Italy) at 37 °C/5% $CO_2$.

For detection of metabolic activity by the MTS assay (Cell Titer 96 Aqueous One Solution, Promega, Madison, WI, USA) and of cell viability and death by the trypan blue dye exclusion test, standard methods were utilized. For detection of SARS-CoV-2 RdRp enzymatic activity, a commercial, fluorometric assay kit from ProFoldin (Hudson, MA, USA) was utilized according to the instructions given. Statistical analysis, $CC_{50}$ and $IC_{50}$ values were calculated using the GraphPad Prism Software V.8.0 for Windows (GraphPad Software Inc., San Diego, CA, USA) from data obtained in three biological replicates. Data were assessed using parametric one-way analysis of variance (ANOVA). The statistical significances were calculated using Bonferroni's Multiple Comparison methods.

## ■ ASSOCIATED CONTENT

### Supporting Information

The Supporting Information is available free of charge at https://pubs.acs.org/doi/10.1021/acsomega.3c04918.

Experimental procedures of synthesized compounds, $^1$H, $^{13}$C, and $^{31}$P NMR spectra of synthesized compounds, tables of the ligand efficiencies and trajectory analyses, and binding pose images of tri- and monophosphate derivatives (PDF)

## ■ AUTHOR INFORMATION


### Corresponding Authors

**Beatrice Macchi** − *Department of Chemical Science and Technology, University of Rome Tor Vergata, 00133 Roma, Italy*; Email: macchi@med.uniroma2.it

**Giulia Morra** − *Biocomputing Lab, SCITEC-Istituto di Scienze e Tecnologie Chimiche CNR, 20131 Milano, Italy*; Email: giulia.morra@scitec.cnr.it

**Paolo Quadrelli** − *Department of Chemistry, University of Pavia, 27100 Pavia, Italy*; orcid.org/0000-0001-5369-9140; Email: paolo.quadrelli@unipv.it

### Authors

**Marco Leusciatti** − *Department of Chemistry, University of Pavia, 27100 Pavia, Italy*

**Francesca Marino-Merlo** − *Department of Chemical, Biological, Pharmaceutical, and Environmental Sciences, University of Messina, 98166 Messina, Italy*

**Antonio Mastino** − *The Institute of Translational Pharmacology, 00133 Roma, Italy*

Complete contact information is available at: https://pubs.acs.org/10.1021/acsomega.3c04918


### Author Contributions

All authors have given approval to the final version of the manuscript.

### Notes

The authors declare no competing financial interest.

In this POC, the syntheses of compounds **4a,b** were conducted according to the well-established methodology as reported in references 16 and 17, leading to the desired products in the racemic forms. The regioisomers **4a,b** were hence fast obtained in a very simple and reliable way. This protocol, in fact, allows for the preparation of consistent amounts of nucleosides at a high level of purity. The optimization of the phosphorylation method required the availability of good amounts of the starting nucleosides to finalize the very last step of the nucleotide synthesis. The enantiomeric resolution has been planned by using chiral amines in a second phase of the study, after a structural evaluation and suitable outlined synthetic changes.



https://doi.org/10.1021/acsomega.3c04918
ACS Omega 2023, 8, 36311−36320

## ■ ACKNOWLEDGMENTS

Financial support by the University of Pavia is gratefully acknowledged. We also thank Steroid S.p.A. and Curia S.r.l. for their financial support to research activities.

## ■ REFERENCES

(1) Lai, C.-C.; Shih, T.-P.; Ko, W.-C.; Tang, H.-J.; Hsueh, P.-R. Severe acute respiratory syndrome coronavirus 2 (SARS-CoV-2) and coronavirus disease-2019 (COVID-19): The epidemic and the challenges. *Int. J. Antimicrob. Agents* **2020**, *55*, 105924 DOI: 10.1016/j.ijantimicag.2020.105924

(2) *WHO announces COVID-19 outbreak a pandemic*. http://www.euro.who.int/en/health-topics/healthemergencies/coronavirus-covid-19/news/news/2020/3/whoannounces-covid-19-outbreak-a-pandemic (accessed Sep 7, 2020)

(3) *Coronavirus (COVID-19) Events As They Happen*; WHO, **2019**; https://www.who.int/emergencies/diseases/novel-coronavirus-2019/events-as-they-happen (accessed Sep 28, 2020).

(4) (a) *COVID-19 Vaccine Development Pipeline; Vaccine Centre, London School of Hygiene and Tropical Medicine* . https://vac-lshtm.shinyapps.io/ncov_vaccine_landscape/ (accessed Sep 7, 2020). (b) *COVID-19 Vaccine Tracker. Lay summary*. https://covid-19tracker.milkeninstitute.org/ (accessed Sep 7, 2020).

(5) Maxmen, A. More than 80 clinical trials launch to test coronavirus treatments. *Nature* **2020**, *578*, 347−348.

(6) (a) Mercorelli, B.; Palù, G.; Loregian, A. Drug Repurposing for Viral Infectious Diseases: How Far Are We? *Trends Microbiol.* **2018**, *26*, 865. (b) Pushpakom, S.; Iorio, F.; Eyers, P. A.; Escott, K. J.; Hopper, S.; Wells, A.; Doig, A.; Guilliams, T.; Latimer, J.; McNamee, C.; Norris, A.; Sanseau, P.; Cavalla, D.; Pirmohamed, M. Drug repurposing: progress, challenges and recommendations. *Nat. Rev. Drug Discovery* **2019**, *18*, 41−58.

(7) Rosa, S. G. V.; Santos, W. C. Clinical trials on drug repositioning for COVID-19 treatment. *Rev. Panam Salud Publica* **2020**, *44*, No. e40.

(8) Gao, Y.; Yan, L.; Huang, Y.; Liu, F.; Zhao, Y.; Cao, L.; Wang, T.; Sun, Q.; Ming, Z.; Zhang, L.; Ge, J.; Zheng, L.; Zhang, Y.; Wang, H.; Zhu, Y.; Zhu, C.; Hu, T.; Hua, T.; Zhang, B.; Yang, X.; Li, J.; Yang, H.; Liu, Z.; Xu, W.; Guddat, L. W.; Wang, Q.; Lou, Z.; Rao, Z. Structure of the RNA-dependent RNA polymerase from COVID-19 virus. *Science* **2020**, *368*, 779 DOI: 10.1126/science.abb7498.

(9) WHO Solidarity Trial Consortium Repurposed Antiviral Drugs for Covid-19 - Interim WHO Solidarity Trial Results. *N Engl. J. Med.* 2020, *384*, 497, DOI: 10.1056/NEJMoa2023184.

(10) Hill, A.; Wang, J.; Levi, J.; Heath, K.; Fortunak, J.*Minimum costs to manufacture new treatments for COVID-19*, 2020. http://viruseradication.com/journal-details/Minimum_costs_to_manufacture_new_treatments_for_COVID-19/.

(11) Picarazzi, F.; Vicenti, I.; Saladini, F.; Zazzi, M.; Mori, M. Targeting the RdRp of Emerging RNA Viruses: The Structure-Based Drug Design Challenge. *Molecules* **2020**, *25*, 5695.

(12) Quadrelli, P. *Modern Applications of Cycloaddition Chemistry*; Elsevier : Amsterdam, 2019; pp. 1−152.

(13) Memeo, M. G.; Quadrelli, P. Generation and trapping of nitrosocarbonyl intermediates. *Chem. Rev.* **2017**, *117*, 2108−2200.

(14) Moggio, Y.; Legnani, L.; Bovio, B.; Memeo, M. G.; Quadrelli, P. Synthesis of novel anthracene derivatives of isoxazolino-carbocyclic nucleoside analogues. *Tetrahedron* **2012**, *68*, 1384−1392.

(15) Zhang, Y.; Jiao, Z.; Xu, W.; Fu, Y.; Zhu, D.; Xu, J.; He, Q.; Cao, H.; Cheng, J. Design, synthesis and properties of a reactive chromophoric/fluorometric probe for hydrogen peroxide detection. *New J. Chem.* **2017**, *41*, 3790−3797.

(16) Memeo, M. G.; Lapolla, F.; Maga, G.; Quadrelli, P. Synthesis and antiviral activity of anthracene derivatives of isoxazolino-carbocyclic nucleoside analogues. *Tetrahedron Lett.* **2015**, *56*, 1986−1990, DOI: 10.1016/j.tetlet.2015.02.114. and references therein.

(17) Quadrelli, P.; Scrocchi, R.; Caramella, P.; Rescifina, A.; Piperno, A. From cyclopentadiene to isoxazoline−carbocyclic nucleosides: a rapid access to biological molecules through nitrosocarbonyl chemistry. *Tetrahedron* **2004**, *60*, 3643−3651.

(18) Ishikura, M.; Murakami, A.; Katagiri, N. First synthesis of 2′,3′-epimino-carbocyclic nucleosides. *Org. Biomol. Chem.* **2003**, *1*, 452−453.

(19) Yoshikawa, M.; Kato, T.; Takenishi, T. Studies of Phosphorylation. III. Selective Phosphorylation of Unprotected Nucleosides. *Bull. Chem. Soc. Jpn.* **1969**, *42*, 3505−3508.

(20) Caton-Williams, J.; Lin, L.; Smith, M.; Huang, Z. Convenient synthesis of nucleoside 5′-triphosphates for RNA transcription. *Chem. Commun.* **2011**, *47*, 8142−8144.

(21) Berger, S.; Braun, S.; Kalinowski, H.-O. *NMR Spectroscopy of the Non-Matallic Elements*; John WileyAnd Sons , 1997.

(22) Peng, Q.; Peng, R.; Yuan, B.; Wang, M.; Zhao, J.; Fu, L.; Qi, J.; Shi, Y. Structural Basis of SARS-CoV-2 Polymerase Inhibition by Favipiravir. *Innovation* **2021**, *2*, No. 100080.

(23) Yin, W.; Mao, C.; Luan, X.; Shen, D.-D.; Shen, Q.; Su, H.; Wang, X.; Zhou, F.; Zhao, W.; Gao, M.; Chang, S.; Xie, Y.-C.; Tian, G.; Jiang, H.-W.; Tao, S.-C.; Shen, J.; Jiang, Y.; Jiang, H.; Xu, Y.; Zhang, S.; Zhang, Y.; Xu, H. E. Structural basis for inhibition of the RNA-dependent RNA polymerase from SARS-CoV-2 by remdesivir. *Science* **2020**, *368*, 1499−1504.

(24) Cannalire, R.; Cerchia, C.; Beccari, A. R.; Di Leva, F. S.; Summa, V. Targeting SARS-CoV-2 Proteases and Polymerase for COVID-19 Treatment: State of the Art and Future Opportunities. *J. Med. Chem.* **2022**, *65*, 2716−2746.

(25) Faita, G.; Leusciatti, M.; Quadrelli, P. Synthesis and biological activity of potential antiviral compounds through 1,3-dipolar cycloadditions; Part 1: general aspects and reactions of azides. *ARKIVOC* **2022**, *part viii*, 19−78.

(26) Faita, G.; Mella, M.; Quadrelli, P. Synthesis and biological activity of potential antiviral compounds through 1,3-dipolar cycloadditions. Part 2: nitrones, nitrile oxides and imines, and other 1,3-dipoles. *ARKIVOC* **2022**, *part viii*, 257−294.



https://doi.org/10.1021/acsomega.3c04918
*ACS Omega* 2023, 8, 36311−36320